Acta Crystallographica Section D
Biological Crystallography
ISSN 0907-4449

X-ray crystal structural analysis of the binding site in the ferric and oxyferrous forms of the recombinant heme dehaloperoxidase cloned from *Amphitrite ornata*

Vesna de Serrano,* Zuxu Chen, Michael F. Davis and Stefan Franzen*

Department of Chemistry, North Carolina State University, Raleigh, NC, USA

Correspondence e-mail: vsserran@ncsu.edu, stefan_franzen@ncsu.edu

Received 29 June 2007
Accepted 4 September 2007

PDB References: wild-type DHP, 2qfk, r2qfksf; C73S mutant DHP, 2qfn, r2qfnsf.

The dehaloperoxidase (DHP) from the terebellid polychaete *Amphitrite ornata* is an enzyme that converts *para*-halogenated phenols to the corresponding quinones in the presence of hydrogen peroxide. Its enzymatic activity is similar to that of heme peroxidases such as horseradish peroxidase, yet it has the structural characteristics of the globin family of proteins, the main functions of which are oxygen transport and storage. In order to investigate the dual function of this hemoglobin peroxidase, the enzyme was expressed in *Escherichia coli* as a recombinant protein in its wild-type form and as a mutant protein in which Cys73 was replaced by a serine residue (C73S). Both the wild-type and mutant proteins were crystallized and their structures were determined at 100 K to a resolution of 1.62 Å. The structure of the wild-type protein demonstrated that it was in the metaquo form, with the heme iron in the ferric oxidation state and the bound water lying 2.2 Å from the heme iron. The structure of the C73S mutant protein was shown to contain a ferrous heme iron with a bound oxygen molecule. The bent bonding geometry of the Fe–O(1)–O(2) adduct results in a hydrogen bond of length 2.8 Å between the second O atom, O(2), of molecular oxygen and $N^{\varepsilon 2}$ of the distal histidine residue (His55) in both subunits contained within the asymmetric unit. This hydrogen-bonding interaction between His55 and the bound diatomic oxygen molecule provides new insight into the catalytic activation of H_2O_2, which is essential for peroxidase activity.

1. Introduction

The enzyme dehaloperoxidase (DHP), first isolated from the terebellid polychaete *Amphitrite ornata*, is a heme-containing peroxidase. Genetic analysis corroborates that DHP is encoded by a gene that has significant sequence homology to the globins of the annelid family (Bailly *et al.*, 2007). Like hemoglobins, DHP is capable of binding diatomic ligands such as molecular oxygen, carbon monoxide and nitric oxide, which bind to the ferrous form of the heme group. In addition, DHP has catalytic properties that are similar to those of horseradish peroxidase (HRP; Ferrari *et al.*, 1999). Quantitative comparisons of the catalytic degradation of halogenated phenols (Belyea *et al.*, 2005; Franzen, Belyea *et al.*, 2006; Franzen, Jasaitis *et al.*, 2006; Chen *et al.*, 1996) demonstrate that DHP has a turnover number that is 12 times lower than HRP, but 13 times greater than myoglobin (Mb) at pH 5.0. HRP is a secretory peroxidase that displays optimal activity at pH < 6.0. DHP, on the other hand, is found in the coelom (fluidic compartment) of *A. ornata* and has a pH optimum of 7.5 (Franzen *et al.*, 2007). Although the different environments complicate comparison, HRP and DHP can both accept a range of halogenated phenols as substrates.

It is not presently understood how DHP switches between its oxygen-binding hemoglobin function and its peroxidase activity. Indeed, this combination of functions is unprecedented in the heme-protein family. Whereas oxygen binding is a reversible process that is common to all ferrous hemoglobins, peroxidase activity requires a ferric resting state. Accordingly, for peroxidase activity, hydrogen peroxide (H_2O_2) binds to ferric heme iron (Fe) to yield compound I according to the reaction

$$P\text{–}Fe^{III}\text{–}H_2O_2 \rightarrow P^{+\cdot}\text{–}Fe^{IV}{=}O + H_2O,$$

where P is the protoporphyrin IX moiety of the heme shown in Fig. 1. Compound I is the oxo heme iron radical cation, $P^{+\cdot}$, that can act as a two-electron oxidant for phenolic substrates according to the overall reaction shown in Fig. 2 at a pH greater than the pK_a of the substrate. We have shown elsewhere that the phenolate form of the substrate is relevant at physiological pH (Franzen *et al.*, 2007).

The X-ray crystallographic structure of DHP isolated from *A. ornata*, first determined by LaCount *et al.* (2000) (PDB code 1ew6), reveals that it has a globin fold but that its heme moiety is located approximately 1.5 Å deeper in the protein than that observed in Mb. The distal histidine is in the same orientation, but is 1.2 Å further from the heme iron than in the Mb structure deposited under PDB code 1a6k (Vojtechovsky *et al.*, 1999). Fig. 1, which is derived from this first structural analysis, displays the heme moiety, the iron, the distal histidine (residue His55) located above the heme plane and the proximal histidine (His89) located below the heme plane. A second DHP structure in complex with the substrate analog 4-iodophenol (PDB code 1ewa) revealed that the substrate analog is bound in an internal binding pocket (LaCount *et al.*, 2000). Given that substrate localization in an internal binding site is unprecedented in globins, this structure suggested that ligand binding might serve as a trigger to switch the protein from its oxygen-carrying role to a catalytic function (Belyea *et al.*, 2005). However, the substrate does not interact strongly with the amino-acid residues of the distal pocket. All the residues in the distal pocket are hydrophobic (Phe21, Val59, Phe35, Phe60), with the exception of the distal histidine His55 and a tyrosine, Tyr38. The hydroxyl group of Tyr38 is sufficiently close to the substrate to form a hydrogen bond with the hydroxyl group of 4-iodophenol.

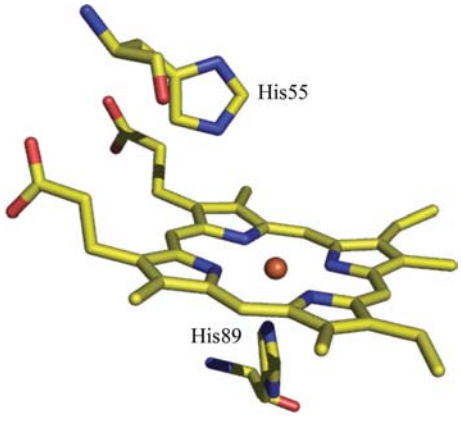

Figure 1
Structure of the heme prosthetic group of DHP relative to the position of the proximal histidine (His89) and distal histidine (His55) located below and above the heme plane, respectively.

The present structural analysis focuses specifically on the ligation of the heme iron in DHP. As is well known, hemoglobins bind oxygen in their ferrous form and are inactive in the ferric oxidation state. Additionally, the ferric irons in methemoglobin and metmyoglobin are six-coordinate when the distal residue (E10) is a histidine (Katz *et al.*, 1994; Royer, 1994; Liu *et al.*, 2001; Vojtechovsky *et al.*, 1999; Yang & Phillips, 1996; Nardini *et al.*, 1995; Della Longa *et al.*, 2003). Ferric peroxidases, which also have a histidine as the distal residue, are usually five-coordinate and thus lack the water molecule bound to the heme iron (Hashimoto *et al.*, 1986; Chouchane *et al.*, 2000; Cheek *et al.*, 1999; Yonetani & Anni, 1987; de Ropp *et al.*, 1991; Andersson *et al.*, 1987; Kuila *et al.*, 1985; Yamazaki *et al.*, 1981; Wang *et al.*, 1990; Kunishima *et al.*, 1996). Strikingly, in the resting state of DHP the ferric form of the heme iron is observed and initial X-ray analysis of native DHP indicated that a water molecule was present in the distal pocket, but it did not appear to be located within bonding distance of the heme iron center (LaCount *et al.*, 2000). Specifically, the Fe—O distances in the A and B subunits were 3.3 and 2.5 Å, respectively. However, spectroscopic experiments (Osborne *et al.*, 2006; Belyea *et al.*, 2006; Nienhaus *et al.*, 2006) suggest that water is bound to the heme iron in the ferric resting state of DHP. Hence, the ligation of the heme in the ferric resting state is still unresolved.

The published X-ray structure of DHP shows the distal histidine residue (His55) in two conformations with nearly equal populations (LaCount *et al.*, 2000). In one of the two conformations His55 is located in the distal cavity, whereas in the second conformation it is positioned away from the distal pocket towards the solvent. This type of conformational variability has precedence in myoglobin, where the distal histidine (His64) assumes the solvent-exposed conformation upon protonation at acidic pH (Yang & Phillips, 1996). Importantly, however, the myoglobin structures that exhibit a solvent-exposed conformation of the distal histidine were obtained below pH 4.5 (Yang & Phillips, 1996), whereas the solvent-exposed conformation of His55 in native DHP was observed at pH 6.5. In addition, the DHP–4-iodophenol complex model shows that His55 is displaced to the solvent-exposed position when the substrate is bound in the distal cavity. Thus, the observation of His55 in a solvent-exposed position and water in the distal pocket, but not bound to the heme iron, may be related.

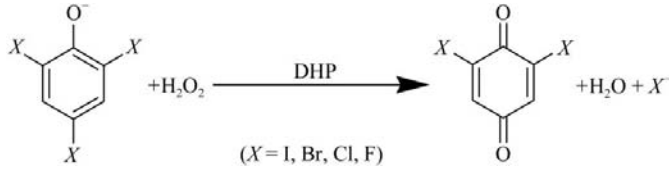

Figure 2
The reaction catalyzed by DHP.

To gain further insight into these issues, we crystallized and solved the structures of wild-type recombinant DHP and the C73S variant. This mutant form of DHP photoreduced in the X-ray beam and thus we were able to obtain a structure of the oxy form of DHP, which yielded further insight into the hydrogen-bonding pattern surrounding His55.

2. Materials and methods

2.1. Purification of recombinant DHP

The C73S mutant DHP was obtained by substituting a serine for a cysteine residue at position 73 using a mutagenesis primer of sequence (5′→3′) GTCGGACGCAAGGGGTAC-CGAATCGGTGGCTCGGTCCGC and its reverse complement. The mutation was generated on the DNA background of four mutated arginine codons in the DNA sequence of DHP, which were introduced to improve expression of the protein in *Escherichia coli* (Belyea *et al.*, 2005). Site-directed mutagenesis was performed using the QuickChange Multi Site-Directed Mutagenesis Kit (Stratagene), as described previously (Belyea *et al.*, 2005).

Genes encoding the wild-type and mutant forms of DHP were cloned into a pET-16b expression vector (Belyea *et al.*, 2005), which was subsequently used to express protein in Rosetta(DE3)pLysS cells. For protein purification, a 50 g cell pellet was resuspended in 100 ml 50 m*M* Tris buffer pH 8.0 supplemented with 100 m*M* NaCl, 1 m*M* EDTA and a protease-inhibitor cocktail (Boehringer Mannheim). The cell suspension was incubated with lysozyme, sonicated and submitted to one cycle of freezing and thawing. After centrifugation to remove cellular debris, the crude extract was subjected to ammonium sulfate fractionation. DHP was precipitated from 50–95% ammonium sulfate. The precipitate was recovered by centrifugation, resuspended in a minimum volume of 20 m*M* Tris pH 8.0 and subjected to dialysis against two changes of the same buffer in order to remove the remaining ammonium sulfate. After subsequent dialysis against 20 m*M* sodium phosphate buffer pH 4.8, followed by brief centrifugation to remove precipitated material, the solution was applied onto an SP Sepharose Fast Flow cation-exchange column using a GE-Pharmacia FPLC system. Protein was eluted with a linear gradient of 0–250 m*M* NaCl in buffer containing 20 m*M* sodium phosphate pH 4.8, 5 m*M* NaN_3 and 5% glycerol. Fractions containing DHP were pooled, concentrated using Millipore centrifugal concentrators and applied onto a HiPrep Sephacryl S-200 column equilibrated with buffer consisting of 50 m*M* Tris pH 5.0, 150 m*M* NaCl and 5% glycerol. The purity of the eluted fractions of DHP was analyzed by SDS–PAGE. The homogeneous fractions were pooled, concentrated and buffer-exchanged to 20 m*M* sodium cacodylate buffer pH 6.5. The protein purity was also assessed by using the ratio of the Soret absorbance at 406 nm to the protein (mostly tryptophan) at 280 nm and DHP protein preparations with A_{406}/A_{280} greater than 3.2 were considered to be pure. UV–visible spectroscopy (UV–Vis) measurement of the Soret band λ_{max} at 406 nm confirmed that both the wild-type enzyme and the C73S mutant protein were isolated in the ferric state (Belyea *et al.*, 2005; Osborne *et al.*, 2006). The integrity of the two proteins was further analyzed by assessing their enzymatic activities toward 2,4,6-tribromophenol (TBP), a natural substrate of DHP (Belyea *et al.*, 2005; Franzen, Belyea *et al.*, 2006; Franzen, Jasaitis *et al.*, 2006).

2.2. Crystallization

The two proteins were crystallized in the ferric form and initial crystallization screening was conducted using commercially available crystal screening kits (Crystal Screens I and II and PEG/Ion Screen; Hampton Research). Both the sitting-drop and hanging-drop methods of vapor diffusion were initially employed at temperatures of 293 and 277 K. After identifying the best conditions, crystals were grown by the hanging-drop method at 277 K. A total drop volume of 6 µl was set up with a 1:1 protein:reservoir solution ratio and the drop was equilibrated against reservoir solution containing 0.2 *M* ammonium sulfate and 26–34% polyethylene glycol 4000. The starting protein concentration was 8 mg ml^{-1}. The pH of the drop solution was 5.9. Diffraction-quality crystals were obtained within one week and ranged in size from 0.2 to 0.7 mm in the largest dimension. They belonged to space group $P2_12_12_1$, with unit-cell parameters a = 60.7, b = 67.6, c = 67.6 Å for the recombinant wild-type protein and a = 57.9, b = 67.1, c = 68.4 Å for the C73S mutant protein. The solvent content for both crystalline lattices was ∼50% and the asymmetric units contained two subunits (Matthews, 1968). For X-ray data collection at low temperatures, the crystals were cryoprotected by brief equilibration in 10 µl 0.2 *M* ammonium sulfate solution containing 32% polyethylene glycol 4000 and 15% polyethylene glycol 400, mounted in a nylon loop and rapidly cryocooled in liquid nitrogen.

2.3. X-ray data collection and structure refinement

X-ray diffraction data for both the wild-type and C73S mutant forms of DHP were collected using a Rigaku RUH3R copper rotating-anode generator (λ = 1.5418 Å) operated at 50 kV and 100 mA with Osmic optics and a Rigaku R-AXIS IV^{++} image-plate detector at the Biomolecular X-ray Crystallography Core Facility, University of North Carolina at Chapel Hill. A full X-ray data set from a single crystal was collected at 100 K using a crystal-to-detector distance of 100 mm and exposure times of 10 min per frame covering 1° oscillations and spanning a range of 150°. All data were processed using the *HKL*-2000 program suite (Otwinowski & Minor, 1997). Each data set extended to a nominal resolution of 1.62 Å. The structures were solved by molecular replacement with the program *Phaser* (McCoy *et al.*, 2005) at 3 Å resolution, using as a search model two polypeptide chains and two heme molecules from the asymmetric unit of the native DHP structure (PDB entry 1ew6; LaCount *et al.*, 2000). In order to eliminate model bias, OMIT maps were constructed with *CNS* (Brünger *et al.*, 1998). Approximately 20 residues in each chain in both the wild-type and C73S mutant structures

Table 1
Data-collection and refinement statistics.

Values in parentheses are for the highest resolution shell.

	Wild-type, recombinant mixed (H_2O, O_2)†	C73S mutant O_2 adduct
Data collection		
Wavelength (Å)	1.5418	1.5418
Space group	$P2_12_12_1$	$P2_12_12_1$
Unit-cell parameters (Å)		
a	60.7	57.9
b	67.6	67.1
c	67.6	68.4
Resolution (Å)	25.62–1.62 (1.66–1.62)	35.0–1.62 (1.68–1.62)
Unique reflections	34161 (2461)	34429 (2289)
Completeness (%)	99.88 (98.66)	99.63 (96.49)
R_{merge}‡ (%)	4.4 (29.5)	5.8 (53.1)
$I/\sigma(I)$	47.7 (6.5)	34.0 (3.0)
Redundancy	5.7	5.7
Refinement		
R_{work}§ (%)	19.1	17.0
R_{free}¶ (%)	23.8	22.4
No. of protein atoms	2391	2434
No. of solvent atoms	275	292
R.m.s.d. from ideal geometry		
Bond lengths (Å)	0.012	0.011
Bond angles (°)	1.3	1.2
Ramachandran plot†† (%)		
Most favored region	94.0	94.8
Additional allowed region	6.0	5.2

† The sixth coordination ligand of the heme Fe is a mixture of water and O_2 in an approximate ratio of 0.75:0.3. ‡ $R_{merge} = \sum_h \sum_i [|I_i(h) - \langle I(h)\rangle|/\sum_h \sum_i I(h)] \times 100$, where $I_i(h)$ is the ith measurement and $\langle I(h)\rangle$ is the weighted mean of all measurements of $I(h)$. § $R_{work} = \sum |F_o - F_c|/\sum F_o \times 100$, where F_o are the observed and F_c the calculated structure factors, respectively. ¶ R_{free} is the R factor for the subset (5%) of reflections selected before and not included in the refinement. †† Calculated using *PROCHECK* (Laskowski *et al.*, 1993).

could be modeled in two conformations and their occupancies were adjusted until there was no significant $F_o - F_c$ density. Using $F_o - F_c$ density contoured at 3σ, 275 water molecules were added to the wild-type model and 292 water molecules were positioned into the mutant structure using *Coot* (Emsley & Cowtan, 2004). The final models were obtained by iterative cycles of model building in *Coot* (Emsley & Cowtan, 2004) and positional and isotropic *B*-factor refinement using *REFMAC*5 (Murshudov *et al.*, 1997) from the *CCP*4 suite of programs (Collaborative Computational Project, Number 4, 1994) and *CNS* (Brünger *et al.*, 1998). Simulated-annealing and composite OMIT maps were constructed using *CNS*. All figures (except Fig. 2) were prepared using *PyMOL* (DeLano, 2002).

The final model for the wild-type structure contained two protein molecules in the asymmetric unit, three sulfate ions, four ammonium ions and 275 water molecules. The final model for the C73S mutant protein structure contained two polypeptide chains, three sulfate ions, two ammonium ions and 292 water molecules. Relevant X-ray data-collection and refinement statistics are summarized in Table 1.

3. Results and discussion

Wild-type DHP expressed in *E. coli* as a recombinant protein produces insoluble precipitates upon prolonged incubation. To test whether the sole surface cysteine (Cys73) plays a role in protein aggregation, it was mutated to a serine residue. Cys73 is located at a distance of approximately 20 Å from the heme iron. This distance was deemed to be sufficiently far that the mutation would not cause significant perturbations in the catalytic properties of the enzyme. Indeed, the C73S mutant protein retained the substrate-binding and catalytic properties of the recombinant wild-type protein (data not shown).

The crystal structures of both the wild-type and C73S mutant forms of DHP were determined for proteins in the Fe^{III} oxidation state as determined by UV–Vis spectra with Soret maxima at 406 nm. Each diffraction data set was collected at 100 K using Cu $K\alpha$ radiation and both structures were refined to a resolution of 1.62 Å, with R factors of 19.1% for the wild-type protein (PDB code 2qfk) and 17.0% for the C73S mutant protein (PDB code 2qfn; Table 1). Both proteins crystallized with two molecules in the asymmetric unit as observed in the original structural analysis of DHP (Zhang *et al.*, 1996). The two subunits have slightly different geometries. For the wild-type enzyme they superimpose with a root-mean-square deviation of 0.27 Å and for the mutant protein structure they superimpose with a root-mean-square deviation of 0.45 Å for all backbone atoms.

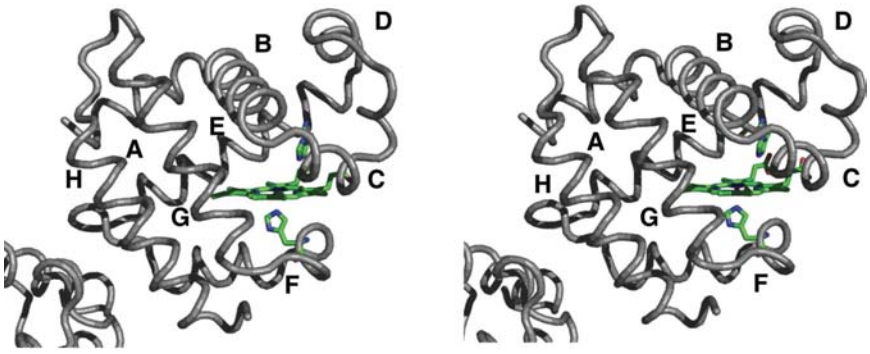

Figure 3
Stereoview of the backbone trace of the wild-type DHP subunit A, shown in ribbon rendering. The eight helices of the structure are labeled A–H according to the globin-fold topology convention. The active-site heme group and the proximal and distal histidine residues are also shown, drawn as green-colored sticks.

3.1. Overall structure of the wild-type and C73S mutant proteins

The structure of the recombinant wild-type DHP consists of a standard myoglobin fold with eight helices (Kendrew *et al.*, 1960). The helical segment, helix C, spanning residues Pro29–Tyr34, adopts a 3_{10}-helical conformation. A backbone trace of the structure of the wild-type protein is presented in Fig. 3, where the eight helices are identified by the letter codes A–H, analogous to the nomenclature for myoglobin (Kendrew *et al.*, 1960). Helix D is two residues shorter in the present structure than that previously reported. As a consequence, the position of His55 in the wild-

Table 2
Comparison of heme-ligand parameters.

The values are tabulated for subunit A of the asymmetric unit.

	Protein form		
	Wild type† (2qfk)	C73S (2qfn)	Original‡ (1ew6)
Fe—His89 $N^{\varepsilon 2}$ (Å)	2.1	2.2	2.3
Fe—His55 $N^{\varepsilon 2}$§ (Å)	4.8	5.1	5.5
Fe—O¶ (Å)	2.2/2.2	2.4/2.2	3.3/2.5
Ligand–His55 (Å)	3.1	O(1) 3.2, O(2) 2.8††	3.6
Fe to pyrrole N plane (Å)	0.04	0.09	0.20
Fe—ligand bend angle‡‡ (°)	—	167.9§§	—
Fe—ligand tilt angle¶¶ (°)	10.9	11	18.3

† Values for the recombinant wild-type DHP structure at 100 K, where the sixth coordination ligand of the heme iron is mixture of water (75%) and O_2 (25%), the mixture being a consequence of partial reduction of the heme iron during X-ray data collection; only parameters for the water ligand are listed in the table. ‡ Compiled from the published structure of DHP determined at room temperature (PDB code 1ew6). § Distance to the His55 conformer located inside the distal cavity. ¶ Fe—O is the distance between the heme iron and ligand oxygen, the ligand being a water molecule in the wild-type and native proteins and an oxygen molecule in the C73S mutant; the two values listed for each structure refer to the distances in subunit A and subunit B, respectively. †† O(1) is the O atom closer to Fe and O(2) is the O atom further from Fe. ‡‡ In subunit B this angle is 145°. §§ The bend angle is the Fe—O—O angle. ¶¶ The tilt angle is the angle between the heme perpendicular and Fe—O (Vangberg *et al.*, 1997).

type metaquo structure solved here is closer to that observed in other hemoglobins and is significantly closer to the heme iron than in the previously solved structure of native DHP (LaCount *et al.*, 2000).

As would be expected, the wild-type and the C73S mutant structures of DHP are nearly identical in the region of the heme-binding site. There are small differences in the two structures, primarily in the subunit-interface region of the molecule, which includes the EF loop where the C73S mutation is located. Both proteins undergo X-ray-induced reduction of the heme iron, but to a different extent. The wild type is reduced only slightly and the structure refines well with a water molecule as a sixth heme iron ligand. The heme center of the C73S mutant undergoes complete reduction, permitting oxygen to bind to its iron.

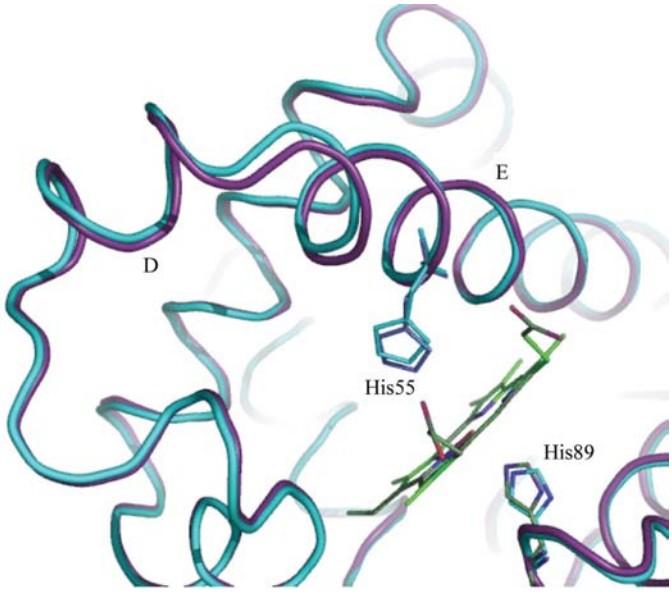

Figure 4
C^{α}-trace superposition of the wild-type DHP (colored purple) and original DHP (colored cyan) structures. Helices D and E are indicated in the figure and the superimposed His55 and His89 residues that illustrate subtle structural differences are shown in stick representation.

3.2. Distal and proximal histidine positions in the structures

Ligands bind to the heme iron of DHP in the distal pocket. Residue His55, referred to as the distal histidine, potentially stabilizes ligands bound to the heme iron through the formation of hydrogen bonds. In the original structure of DHP, His55 was displaced from the distal pocket when the substrate bound in the internal binding site (LaCount *et al.*, 2000). In the structures presented here, the conformation of His55 is closer to the heme iron. Indeed, in our structure of the wild-type metaquo DHP form, the distal histidine is located 0.75 Å closer to the heme iron (Table 2 and Fig. 4). The distance from the distal histidine to the heme iron in the structure presented here is close to the distance observed in myoglobin at neutral pH (PDB entry 1a6k; Vojtechovsky *et al.*, 1999). In the structure of the C73S mutant protein (PDB code 2qfn), which has an oxygen molecule bound in the distal pocket, the His55 residue is a little further removed from the heme iron, as shown in the superimposed active sites of the two proteins in Fig. 5. As a consequence, there is a hydrogen bond between His55 $N^{\varepsilon 2}$ and the O(2) atom of the oxygen molecule (see below). The distal histidine does not exhibit a solvent-exposed conformation based on OMIT maps where His55 is removed from the calculations. The electron density observed in the OMIT map could accommodate only one water molecule instead of a histidine residue. Under the present crystallization conditions, His55 exhibits a single conformation, which is inside the distal pocket in both the wild-type and C73S mutant protein structures.

The proximal histidine His89 is the fifth coordination ligand of the heme iron in DHP and is positioned at a distance of 2.1 Å from the heme iron in the wild-type protein and at a distance of 2.2 Å in the C73S mutant protein (Table 2 and Fig. 5). In the original structure of DHP, the bond length of the proximal histidine $N^{\varepsilon 2}$ to the iron was observed to be 2.3 Å (Table 2). It is believed that the protein environment on the proximal side of the heme influences the reactivity of the heme iron towards *trans* ligands. The distances observed in the structures presented here agree with those found in globins (Vojtechovsky *et al.*, 1999). The Fe–His distance can be shorter in peroxidases (Bonagura *et al.*, 2003), which may arise from strong hydrogen bonding of a neighboring aspartate to the proximal histidine (Spiro *et al.*, 1990), leading to an Asp-His-Fe triad on the proximal side (Goodin & McRee, 1993). This interaction leads to an even shorter Fe—$N^{\varepsilon 2}$ bond length of 2.1 Å in cytochrome *c* peroxidase (Bonagura *et al.*, 2003).

3.3. Coordination geometries of the ligands in the two forms of DHP

The differences in the distal and proximal histidine positions discussed above appear to correlate with a six-coordinate

heme iron in both the wild-type and C73S protein structures. In the wild-type model, shown in Fig. 6(*a*), a water molecule is positioned in the distal pocket at a coordination distance of 2.2 Å from the heme iron in both the A and B subunits. In the original DHP structure, the waters present in the distal pocket are at nonbonding distances of 3.3 and 2.5 Å, respectively, in subunits A and B (Table 2). This Fe—O distance is most likely to arise from subtle variations in crystallization conditions that affect the distal pocket. The Fe—O bond length of 2.2 Å in the wild-type structure presented here is consistent with a chemical bond, while the longer distance in the first DHP structure is most likely to indicate that water is trapped in the distal pocket but not bound to the heme iron. The six-coordinate metaquo adduct observed here is consistent with the structures of all ferric myoglobins and hemoglobins that have a distal histidine. Moreover, magnetic circular dichroism (Osborne *et al.*, 2006), resonance Raman spectroscopy (Belyea *et al.*, 2006) and UV–Vis titrations (Nienhaus *et al.*, 2006) are also consistent with the coordination of water as observed in this investigation.

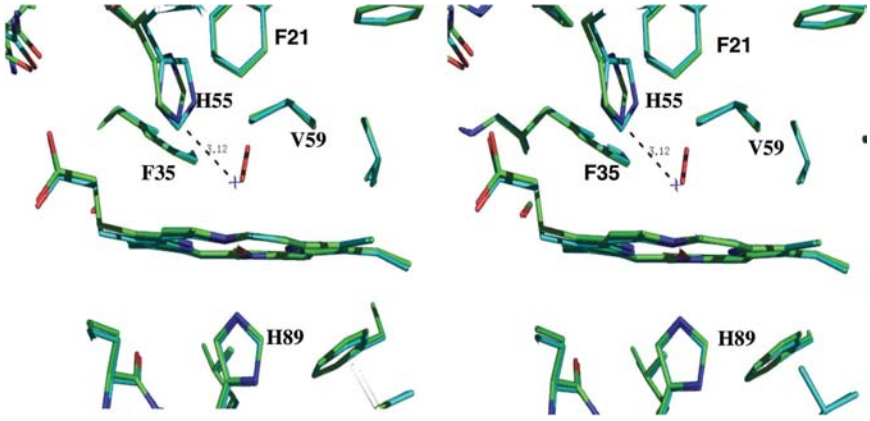

Figure 5
Stereoview of an overlay of the distal pocket region for the wild-type recombinant enzyme (colored green) and the O_2-ligated form of the C73S mutant protein (colored cyan). The figure emphasizes the differences in the conformation of His55 in the two superimposed structures of subunit A. The indicated hydrogen bond between His55 $N^{\epsilon 2}$ and the water molecule bound to the heme iron in the wild-type protein has an N—O distance of 3.1 Å.

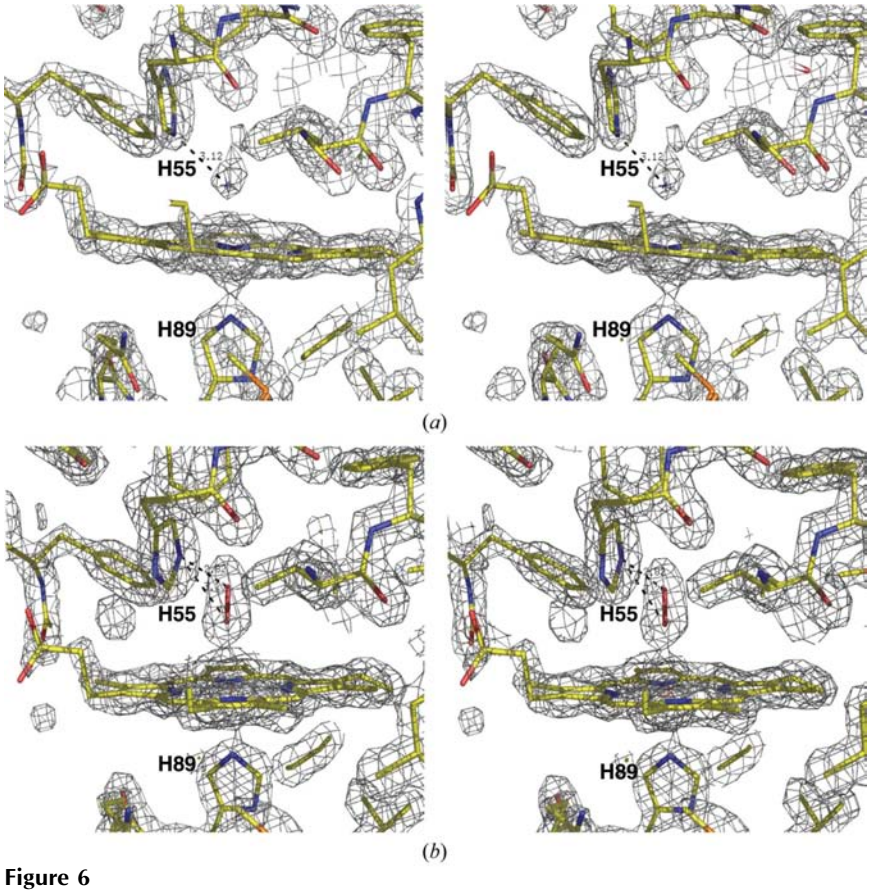

Figure 6
Stereo representation of electron-density maps ($2F_o - F_c$) for the wild-type protein (*a*) and the O_2 complex of the C73S mutant form of DHP (*b*). The maps were contoured at 1.5σ for the wild-type enzyme and at 1.7σ for the C73S–oxygen complex. The coordinates shown correspond to subunit A.

There was clearly more electron density observed above the heme iron in the distal pocket in the C73S mutant protein compared with the wild-type structure. It is most likely that the C73S mutant protein was photoreduced during X-ray data collection (Berglund *et al.*, 2002; de Sanctis *et al.*, 2004; Schlichting *et al.*, 2000; Sjorgren & Hajdu, 2001; Fedorov *et al.*, 2003; Bolognesi *et al.*, 1999). While the wild-type enzyme had a minority population of reduced heme iron, reduction was virtually complete in the C73S mutant protein (Table 1). Composite OMIT $2F_o - F_c$ maps were calculated in *CNS* by omitting 5% of the model for 20 cycles of simulated-annealing refinement steps with a starting temperature of 4000 K. These maps revealed differences in the ligation geometries between the wild-type and C73S mutant proteins. The results shown in Fig. 6(*b*) indicate that diatomic oxygen is ligated to the heme iron in the C73S mutant protein structure.

3.4. Mechanistic significance of distal histidine hydrogen bonding

The distal histidine His55 forms hydrogen bonds to both water and O_2 in the structures reported here. In the wild-type model, His55 forms a weak hydrogen bond to the water ligand bound to the heme iron such that $N^{\delta 1}$ is positioned at a hydrogen-bonding distance of 3.0 Å from the hydroxyl of the Tyr38 residue. This hydrogen bond might be important for reactivity since it may regulate H_2O displacement from the heme iron when either substrate or H_2O_2 binds as part of the

Table 3
Comparison of the distances of His55 to the heme Fe ligand and the hydroxyl group of Tyr38 in the wild-type and C73S mutant protein structures.

Values in bold emphasize relevant hydrogen-bonding distances; values are listed for subunit A.

	His55 distances (Å)			
	Wild-type (2qfk)		C73S (2qfn)	
	$N^{\delta1}$	$N^{\varepsilon2}$	$N^{\delta1}$	$N^{\varepsilon2}$
Ligand†	4.9	**3.1**	O(1) 4.5, O(2) 4.6	O(1) **3.2**, O(2) **2. 8**
Tyr38 OH	**3.0**	4.8	4.4	4.7

† For the wild-type recombinant structure the values are listed for water as a ligand; for the C73S mutant of DHP the sixth coordination ligand of the heme iron is O_2.

peroxidase catalytic cycle. For example, if the substrate binds first then it could displace His55 to the solvent-exposed conformation observed in the original DHP structure, thereby allowing the binding of H_2O_2. It is possible that H_2O is a gatekeeper that regulates the initiation of the catalytic cycle. This behavior would be analogous to the displacement of water in the catalytic cycle of cytochrome $P450_{cam}$ (Sligar & Gunsalas, 1976).

The hydrogen bond to the diatomic oxygen in the C73S structure is stronger than the hydrogen bond to water. The oxygen molecule is bent and the Fe—O(1)—O(2) angle is 168° in subunit A and 144° in subunit B. There is also a small tilt angle [defined as the angle between the heme perpendicular and the Fe—O(1) bond (Vangberg *et al.*, 1997)] of 11° and 6°, respectively. Both O atoms of the molecule can form hydrogen bonds to $N^{\varepsilon2}$ of the distal histidine His55, with distances of 2.8 Å for O(2) and a weaker 3.2 Å bond distance for O(1) in subunit A (Table 2). In this orientation, His55 $N^{\delta1}$ is no longer within hydrogen-bonding distance of Tyr38, but instead faces the solvent. In mechanistic terms, this new interaction of His55 (by analogy, also likely to occur with H_2O_2) could facilitate closer contacts of Tyr38 with the substrate in the course of the enzymatic activity of DHP, while at the same time allowing His55 to move into a position that straddles the two O atoms of bound H_2O_2. This conformation of His55 is consistent with its role as an acid/base catalyst needed for the activation of H_2O_2 to form compound I (Poulos & Kraut, 1980). The catalytic step involves abstracting a hydrogen from O(1) and transferring it to O(2) as indicated below:

$$\begin{aligned} &P\text{–}Fe^{III}\text{–}H\text{–}O(1)\text{–}O(2)\text{–}H + His\text{–}N^{\varepsilon2} \\ &\quad\rightarrow P\text{–}Fe^{III}\text{–}O(1)\text{–}O(2)\,\text{–}H^{-} + His\text{–}N^{\varepsilon2}\text{–}H^{+} \\ &\quad\rightarrow P\text{–}Fe^{III}\text{–}O(1)\,\text{–}O(2)\,\text{–}H_2 + His\text{–}N^{\varepsilon2} \\ &\quad\rightarrow P^{+\cdot}\text{–}Fe^{IV}\text{=}O(1) + O(2)\text{–}H_2 + His\text{–}N^{\varepsilon2}. \end{aligned}$$

The transfer leads to heterolytic bond cleavage and the formation of compound I. The distances from both Tyr38 and the heme iron ligand to the distal histidine His55 are listed in Table 3 to emphasize the differences between the wild-type and C73S mutant protein structures.

Normally, peroxidases have an arginine residue that resides near the distal histidine that acts to stabilize the proton transfer required to promote heterolytic bond cleavage. Since this arginine is missing in DHP, the observed hydrogen bond may account for the activation of the peroxy intermediate to form compound I. We can infer that Tyr38 is a critical residue in this process since it changes from hydrogen bonding to His55 (substrate-free) to hydrogen bonding to the substrate itself (substrate-bound) as evident in the first DHP crystal structure (LaCount *et al.*, 2000). Both the strong hydrogen bond in the oxy form and the water bound in the ferric form, which is the peroxidase resting state, are new features that have not been observed previously for this enzyme.

4. Conclusion

The hypothesis that His55 activates bound H_2O_2 in DHP is strengthened by the structural data presented here. However, there is an apparent contradiction in this hypothesis if one considers both solution reactivity and the X-ray crystal structures. The first DHP structure showed that His55 was displaced to a solvent-exposed conformation more than 9 Å from the heme iron when the substrate was bound in the distal pocket (LaCount *et al.*, 2000). However, mechanistic data indicate that the enzyme is inactivated if H_2O_2 is added more than 30 s prior to the substrate (Belyea *et al.*, 2005). In order for His55 to catalyze the formation of compound I it must be in the distal pocket, yet according to the original model it will be displaced when substrate is bound. There are three possibilities that can account for this apparent inconsistency. The first possibility is that His55 does not activate H_2O_2, but rather the phenolate oxygen activates bound H_2O_2 (Franzen *et al.*, 2007). However, this hypothesis can only explain the reactivity when the pH is greater than the pK_a, which is not relevant for the crystallization conditions of the structures presented here. Stopped-flow data show that DHP has significant peroxidase activity even when the pH is less than the pK_a of the substrate (Belyea *et al.*, 2005). The second possibility is that the substrate always binds to the enzyme within 30 s of activation. This seems unlikely unless the substrate first interacts on the exterior of the enzyme in a priming step that serves as a trigger for the onset of peroxidase function. Without such a step DHP would wastefully bind H_2O_2 and be rapidly inactivated. The third possibility is that the substrate binds to an external site. This binding could either be a priming event as suggested above or it could be that oxidation takes place at an external binding site near the heme edge as observed for other heme peroxidases (Ator & de Montellano, 1987). The present structure shows the possible interactions of His55 with a bound diatomic molecule and thus our current data support the third hypothesis at low pH and perhaps more generally. The resolution of these issues will require additional NMR and X-ray crystallographic studies, which are presently under way.

We acknowledge financial support for this work from Army Research Office Grant 52278-LS. We thank Dr Robert Rose, Department of Molecular and Structural Biochemistry at NCSU for his help, guidance and discussions during this

project. We also thank Dr Laurie Betts of the UNC Biomolecular X-ray Crystallography Core Facility for assistance in the X-ray data collection and analysis. We thank Dr David Lambright for essential advice on crystallization conditions and analysis.

References

Andersson, L. A., Renganathan, V., Loehr, T. M. & Gold, M. H. (1987). *Biochemistry*, **26**, 2258–2263.

Ator, M. A. & de Montellano, P. R. O. (1987). *J. Biol. Chem.* **262**, 1542–1551.

Bailly, X., Chabasse, C., Hourdez, S., Dawilde, S., Martial, S., Moens, L. & Zal, F. (2007). *FEBS J.* **274**, 2641–2652.

Belyea, J., Belyea, C. M., Lappi, S. & Franzen, S. (2006). *Biochemistry*, **45**, 14275–14284.

Belyea, J., Gilvey, L. B., Davis, M. F., Godek, M., Sit, T. L., Lommel, S. A. & Franzen, S. (2005). *Biochemistry*, **44**, 15637–15644.

Berglund, G. I., Carlsson, G. H., Smith, A. T., Szoke, H., Henriksen, A. & Hajdu, J. (2002). *Nature (London)*, **417**, 463–468.

Bolognesi, M., Rosano, C., Losso, R., Borassi, A., Rizzi, M., Wittenberg, J. B., Boffi, A. & Ascenzi, P. (1999). *Biophys. J.* **77**, 1093–1099.

Bonagura, C. A., Bhaskar, B., Shimizu, H., Li, H. Y., Sundaramoorthy, M., McRee, D. E., Goodin, D. B. & Poulos, T. L. (2003). *Biochemistry*, **42**, 5600–5608.

Brünger, A. T., Adams, P. D., Clore, G. M., DeLano, W. L., Gros, P., Grosse-Kunstleve, R. W., Jiang, J.-S., Kuszewski, J., Nilges, M., Pannu, N. S., Read, R. J., Rice, L. M., Simonson, T. & Warren, G. L. (1998). *Acta Cryst.* D**54**, 905–921.

Cheek, J., Mandelman, D., Poulos, T. L. & Dawson, J. (1999). *J. Biol. Inorg. Chem.* **4**, 64–72.

Chen, Y. P., Woodin, S. A., Lincoln, D. E. & Lovell, C. R. (1996). *J. Biol. Chem.* **271**, 4609–4612.

Chouchane, S., Lippai, I. & Magliozzo, R. S. (2000). *Biochemistry*, **39**, 9975–9983.

Collaborative Computational Project, Number 4 (1994). *Acta Cryst.* D**50**, 760–763.

DeLano, W. L. (2002). *The PyMOL Molecular Graphics System.* DeLano Scientific, San Carlos, CA, USA.

Della Longa, S., Arcovito, A., Benefatto, M., Congiu-Castellano, A., Girasole, M., Hazemann, J. L. & Lo Bosco, A. (2003). *Biophys. J.* **85**, 549–558.

Emsley, P. & Cowtan, K. (2004). *Acta Cryst.* D**60**, 2126–2132.

Fedorov, R., Ghosh, D. K. & Schlichting, I. (2003). *Arch. Biochem. Biophys.* **409**, 25–31.

Ferrari, R. P., Laurenti, E. & Trotta, F. (1999). *J. Biol. Inorg. Chem.* **4**, 232–237.

Franzen, S., Belyea, J., Gilvey, L. B., Davis, M. F., Chaundhary, C. E., Sit, T. L. & Lommel, S. (2006). *Biochemistry*, **45**, 9085–9094.

Franzen, S., Gilvey, L. B. & Belyea, J. (2007). *Biochim. Biophys. Acta*, **1774**, 121–130.

Franzen, S., Jasaitis, A., Belyea, J., Brewer, S. H., Casey, R., MacFarlane, A., W., Stanley, R. J., Vos, M. H. & Martin, J.-L. (2006). *J. Phys. Chem. B*, **110**, 14483–14493.

Goodin, D. B. & McRee, D. E. (1993). *Biochemistry*, **32**, 3313–3324.

Hashimoto, S., Teraoka, J., Inubushi, T., Yonetani, T. & Kitagawa, T. (1986). *J. Biol. Chem.* **261**, 11110–11118.

Katz, D. S., White, S. P., Huang, W., Kumar, R. & Christianson, D. W. (1994). *J. Mol. Biol.* **244**, 541–553.

Kendrew, J. C., Dickerson, R. E., Strandberg, B. E., Hart, R. G., Davies, D. R., Phillips, D. C. & Shore, V. C. (1960). *Nature (London)*, **185**, 422–427.

Kuila, D., Tien, M., Fee, J. A. & Ondrias, M. R. (1985). *Biochemistry*, **24**, 3394–3397.

Kunishima, N., Amada, F., Fukujama, K., Kawamoto, M., Maesunaga, T. & Matsubara, H. (1996). *FEBS Lett.* **378**, 291–294.

LaCount, M. W., Zhang, E., Chen, Y. P., Han, K., Whitton, M. M., Lincoln, D. E., Woodin, S. A. & Lebioda, L. (2000). *J. Biol. Chem.* **275**, 18712–18716.

Laskowski, R. A., MacArthur, M. W., Moss, D. S. & Thornton, J. M. (1993). *J. Appl. Cryst.* **26**, 283–291.

Liu, X.-Z., Li, S.-L., Jing, H., Liang, Y.-H., Hua, Z.-Q. & Lu, G.-Y. (2001). *Acta Cryst.* D**57**, 775–783.

McCoy, A. J., Grosse-Kunstleve, R. W., Storoni, L. C. & Read, R. J. (2005). *Acta Cryst.* D**61**, 458–464.

Matthews, B. W. (1968). *J. Mol. Biol.* **33**, 491–497.

Murshudov, G. N., Vagin, A. A. & Dodson, E. J. (1997). *Acta Cryst.* D**53**, 240–255.

Nardini, M., Tarricone, C., Rizzi, M., Lania, A., Desideri, A., De Sanctis, G., Coletta, M., Petruzzelli, R., Ascenzi, P., Coda, A. & Bolognesi, M. (1995). *J. Mol. Biol.* **247**, 459–465.

Nienhaus, K., Deng, P., Belyea, J., Franzen, S. & Nienhaus, G. U. (2006). *J. Phys. Chem. B*, **110**, 13264–13276.

Osborne, R. L., Sumithran, S., Coggins, M. K., Chen, Y.-P., Lincoln, D. E. & Dawson, J. H. (2006). *J. Inorg. Biochem.* **100**, 1100–1108.

Otwinowski, Z. & Minor, W. (1997). *Methods Enzymol.* **276**, 307–326.

Poulos, T. L. & Kraut, J. (1980). *J. Biol. Chem.* **255**, 575–580.

Ropp, J. S. de, LaMar, G. N., Wriishi, H. & Gold, M. H. (1991). *J. Biol. Chem.* **266**, 15001–15008.

Royer, W. E. Jr (1994). *J. Mol. Biol.* **235**, 657–681.

Sanctis, D. de, Dewilde, S., Pesce, A., Moens, L., Ascenzi, P., Hankeln, T., Burmester, T. & Bolognesi, M. (2004). *J. Mol. Biol.* **336**, 917–927.

Schlichting, I., Berendzen, J., Chu, K., Stock, A. M., Maves, S. A., Benson, D. E., Sweet, R. M., Ringe, D., Petsko, G. A. & Sligar, S. G. (2000). *Science*, **287**, 1615–1622.

Sjorgren, T. & Hajdu, J. (2001). *J. Biol. Chem.* **276**, 13072–13076.

Sligar, S. G. & Gunsalas, I. C. (1976). *Proc. Natl Acad. Sci. USA*, **73**, 1078–1081.

Spiro, T. G., Smulevich, G. & Su, G. (1990). *Biochemistry*, **29**, 4497–4508.

Vangberg, T., Bocian, D. F. & Ghosh, A. (1997). *J. Biol. Inorg. Chem.* **2**, 526–530.

Vojtechovsky, J., Chu, K., Berendzen, J., Sweet, R. M. & Schlichting, I. (1999). *Biophys. J.* **77**, 2153–2174.

Wang, J., Mauro, M., Edwards, S. L., Oatley, S. J., Fishel, L. A., Ashford, V. A., Xuong, N.-H. & Krout, J. (1990). *Biochemistry*, **29**, 7160–7173.

Yamazaki, I., Tamura, M. & Nakajima, R. (1981). *Mol. Cell. Biochem.* **40**, 143–153.

Yang, F. & Phillips, G. N. (1996). *J. Mol. Biol.* **256**, 762–774.

Yonetani, T. & Anni, H. (1987). *J. Biol. Chem.* **262**, 9547–9554.

Zhang, E., Chen, Y. P., Roach, M. P., Lincoln, D. E., Lovell, C. R., Woodin, S. A., Dawson, J. H. & Lebioda, L. (1996). *Acta Cryst.* D**52**, 1191–1193.